Probing the Oceanic Precipitable Water Vapor Evolution Characteristics during the 2020 Tropical Cyclone Maysak using the GNSS Radio Occultation and Satellite Microwave Radiometry Data

Shiwei Yu[1], **Zhizhao Liu**[2]

Abstract A tropical cyclone (TC) is a rapidly rotating storm system with complex weather phenomena, such as powerful winds, heavy rainstorms, and damaging thunderstorms. It brings enormous effects on human lives and properties over the coastal area. Moreover, the intensity of TCs is showing an increasing trend with global warming. Therefore, monitoring tropical cyclones, including the atmospheric evolution characteristics, is scientifically and practically meaningful. The Global Navigation Satellite System (GNSS) radio occultation (RO) is a powerful tool to study the atmosphere evolution during the TC period. Much more RO sounding data can be utilized than before with the completion of the new generation six-satellite Constellation Observing System for Meteorology Ionosphere and Climate (COSMIC-2) in 2019. In this study, we analyzed the precipitable water vapor (PWV) in the upper atmosphere between 1.6 km and 40.0 km. We classified the region around the TC eye center into five bands according to the distance to the TC eye center: band 1 for the region with a radius of 0-200 km from TC eye center; band 2 for 200-400 km; band 3 for 400-600 km; band 4 for 600-800 km; and band 5 for 800-1000 km. The PWV within the band 1 showed an evident increase from August 28 with a value of ~39.5 kg/m^2 to September 1, 2020 with a value of ~43.6 kg/m^2, when the TC became increasingly intensified. While the PWV in bands 2 to 5 showed a decreasing trend during this period. The mean PWV gradient was -2.47 $kg \cdot m^2 \cdot (100km)^{-1}$ from band 1 to band 2, -2.27 $kg \cdot m^2 \cdot (100km)^{-1}$ from

[1] Shiwei Yu
Department of Land Surveying & Geo-Informatics (LSGI), The Hong Kong Polytechnic University (PolyU), Hong Kong, P.R. China
Research Institute for Sustainable Urban Development, The Hong Kong Polytechnic University (PolyU), Hong Kong, P. R. China

[2] Zhizhao Liu (✉)
Department of Land Surveying & Geo-Informatics (LSGI), The Hong Kong Polytechnic University (PolyU), Hong Kong, P.R. China
Research Institute for Sustainable Urban Development, The Hong Kong Polytechnic University (PolyU), Hong Kong, P. R. China
e-mail: lszzliu@polyu.edu.hk

band 2 to band 3, -1.17 $kg \cdot m^2 \cdot (100km)^{-1}$ from band 3 to band 4, and -1.16 $kg \cdot m^2 \cdot (100km)^{-1}$ from band 4 to band 5. We also analyzed PWV data from altimetry satellites and found that symmetric spatial gradient of PWV can be apparently observed. These findings can help us further understand the atmospheric evolution characteristics over ocean during the TC period, thus improve the forecast reliability and accuracy.

Keywords: Precipitable Water Vapor, GNSS Radio Occultation, Altimetry Satellite, Tropical Cyclone

1 Introduction

A tropical cyclone (TC) is a complex storm system characterized by a low-pressure center, powerful winds, and a spiral arrangement of thunderstorms [1]. TCs are one of the weather disasters with a destructive nature during and after the landfall. TC landfall accompanying strong winds and intense rainfall poses severe risks to the lives and properties of coastal regions. The annual global damage from TCs is approximately US$ 26 billion [2], and the annual global fatalities from TCs is around 8,000 on average [3]. Moreover, researchers have found that the intensity of TCs is showing an increasing trend due to global warming [4]. Therefore, a good understanding of TC's mechanism can help to improve the TC forecasting accuracy and reduce property and life losses.

The meteorological parameters, such as temperature, atmosphere pressure, and relative humidity, play a fundamental role in the TC forecasting models [5]. The primary observation source of these parameters is remote sensing meteorological satellites, such as Fengyun meteorological satellites of the National Satellite Meteorological Center (NSMC) of China [6]. However, the main drawbacks of this technique are the low temporal resolution, e.g. ~12 hours, and the low spatial resolution e.g. 0.25°×0.25° [7]. In addition, remote sensing satellites seldom provide meteorological observations in a vertical profile.

The global navigation satellite system (GNSS) radio occultation (RO) provides us with an opportunity to understand atmospheric dynamics from the vertical aspect. For instance, Healy et al. [8] utilized GNSS RO data to study zonal winds in the tropical stratosphere at different pressure levels. In addition, numerous studies showed that GNSS RO data can help to improve the accuracy of TC forecasts [9, 10]. With the completion of the second-generation Constellation Observing System for Meteorology Ionosphere and Climate (COSMIC-2) mission in 2019, ~5,000 sounding can be observed every day globally, more than ~3 times compared with the first-generation COSMIC, i.e. ~1,500 soundings [11]. Besides the GNSS RO technique, MWR instrument onboard altimetry satellites is another powerful tool to facilitate atmospheric dynamics research. Different from the MWR instrument

onboard the remote sensing satellites, the MWR onboard altimetry satellites can measure the precipitable water vapor (PWV) in the atmosphere at the nadir points with high spatial and temporal resolutions, e.g. 20 km and 1 second intervals between sounding points in Sentinel-3 mission [12].

Taking advantage of these RO and altimetry satellite techniques, we studied the atmospheric dynamics during the 2020 tropical cyclone Maysak in the western North Pacific Ocean. The data and methodology are introduced in Section 2. In Section 3, the PWV variations observed by the GNSS RO soundings and MWR soundings from altimetry satellites is presented. The conclusions are summarized in Section 4.

2 Data and Methodology

In this section, the TC information and PWV retrieval method from GNSS RO and altimetry satellites are introduced.

2.1 The 2020 TC Maysak

Maysak formed as a tropical depression over the western North Pacific about 1,050 km east-northeast of Manila, Philippines, on the afternoon of August 28, 2020. It intensified into a typhoon on August 30 and moved northward. It further intensified into a super typhoon on the night of August 31 and passed through the Ryukyu Islands, Japan. Maysak reached its peak intensity on the morning of September 1. The sustained wind speed near its center was estimated to be ~ 195 km/h. Maysak then moved north-northeastward and swept across the East China Sea. It made landfall over the south of the Korean Peninsula on the afternoon of September 2 [13]. The track of the Maysak is presented in Fig. 1, based on the data retrieved from the International Best Track Archive for Climate Stewardship (IBTrACS) of the National Oceanic and Atmospheric Administration (NOAA) [14].

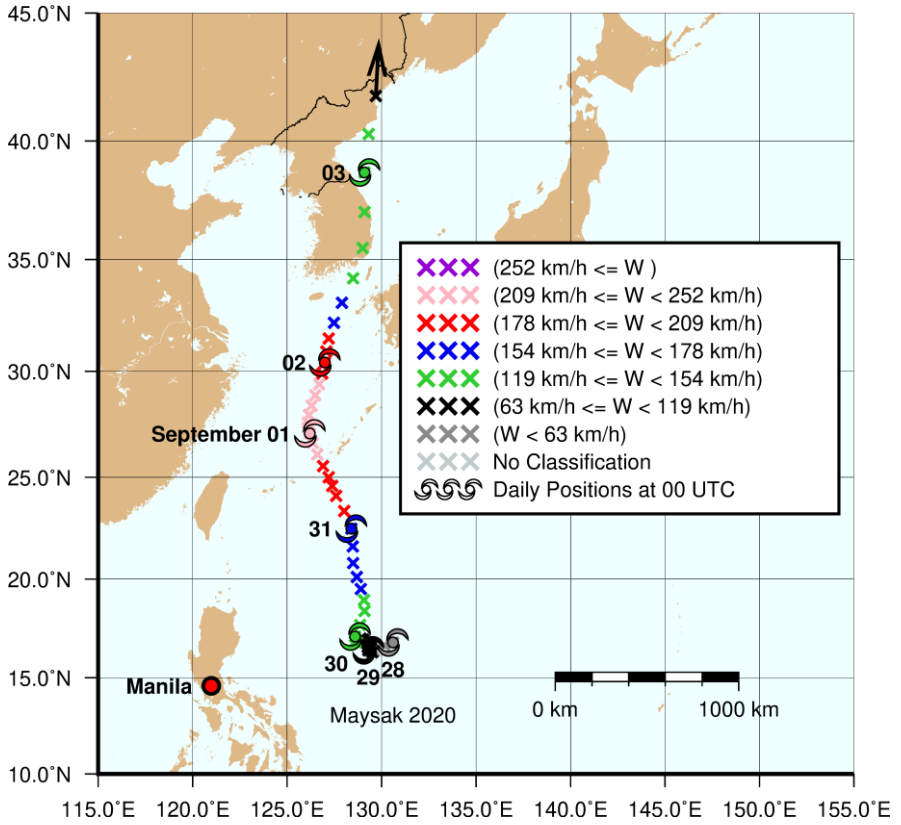

Fig. 1 Track of the 2020 TC Maysak, for which the TC center positions were presented every 3 hours, and the date marked beside the track denotes the TC position at 00 UTC of that given day. The color denotes different TC categories according to the 1-minute maximum sustained surface wind speed defined by the National hurricane center of the NOAA (https://www.nhc.noaa.gov/pdf/sshws.pdf)

2.2 PWV from GNSS RO Sounding

To investigate the PWV variation during the TC period, we calculated the PWV based on the atmospheric parameters from each GNSS RO profile. The PWV can be expressed as [15]:

$$PWV = \frac{1}{g}\int_{Pb}^{Pt} qdP \quad (1)$$

$$g = 9.784 \cdot (1 - 0.00266 \cdot cos2\varphi - 0.00028 \cdot H) \quad (2)$$

$$q = \frac{0.62198 \cdot e}{P - e \cdot (1 - 0.62198)} \quad (3)$$

where g is the gravitational acceleration in m/s^2. It can be expressed as a function of latitude φ in the unit of radians and height H in the unit of km. Pb and Pt in the unit of Pa are the pressure at the bottom and top of the atmosphere profile. q is the specific humidity. The specific humidity q at a pressure level of P in the unit of Pa

can be calculated from the water vapor pressure e in the unit of Pa at the corresponding pressure level.

In this study, data from multiple GNSS RO missions are used, including (1) COSMIC-2 jointly developed by the Nation Space Organization (NSPO) of Taiwan, China, and the NOAA and the United States Air Force (USAF); (2) meteorological operational satellites such as Metop-A, Metop-B, and Metop-C developed by the European Space Agency; (3) Korea Multi-Purpose Satellite-5 (KOMPASAT5) designed by the Korea Aerospace Research Institute; (4) PAZ of the Spanish National Earth Observation Programme; (5) TerraSAR-X (TSX) and TanDEM-X (TDX) managed by the German Aerospace Center.

2.3 PWV from Altimetry Satellites

Altimetry satellites were often equipped with MWR instrument to remove the atmospheric delay caused by the water vapor in the range measurement [16]. From the other aspect, the MWR measurements can be utilized to study the water vapor variation. In this study, we analyzed the PWV variation from four altimetry satellites, including SARAL, Jason-3, Sentinel 3A, and Sentinel 3B.

3 Results

In this section, we investigated the PWV retrieved from both the GNSS RO missions and altimetry satellite missions during the TC Maysak.

3.1 PWV Variation based on GNSS RO Soundings

PWV of the GNSS RO sounding profiles can be calculated by integrating specific humidity from the bottom to top sounding points. Due to the low signal power and the terrain features [11], the penetration depths are different in different GNSS RO sounding profiles. Zhu et al. [17] found that the PWV in the lower troposphere (0–1.6 km) has almost no change during the whole life cycle of TC but the PWV above the altitude of 1.6 km showed a significant increase with the effect of TCs. To get a consistent comparison of PWV from all GNSS RO profiles, we calculated the PWV between altitudes of 1.6 km and 40.0 km. For every day from August 28 to September 2, PWV at each GNSS RO sounding point within a radius of 1,000 km from the TC center is shown in Fig. 2. Examining the colors of the dots, it can be seen that PWV closer to the TC center generally had a higher level than that far from the TC center.

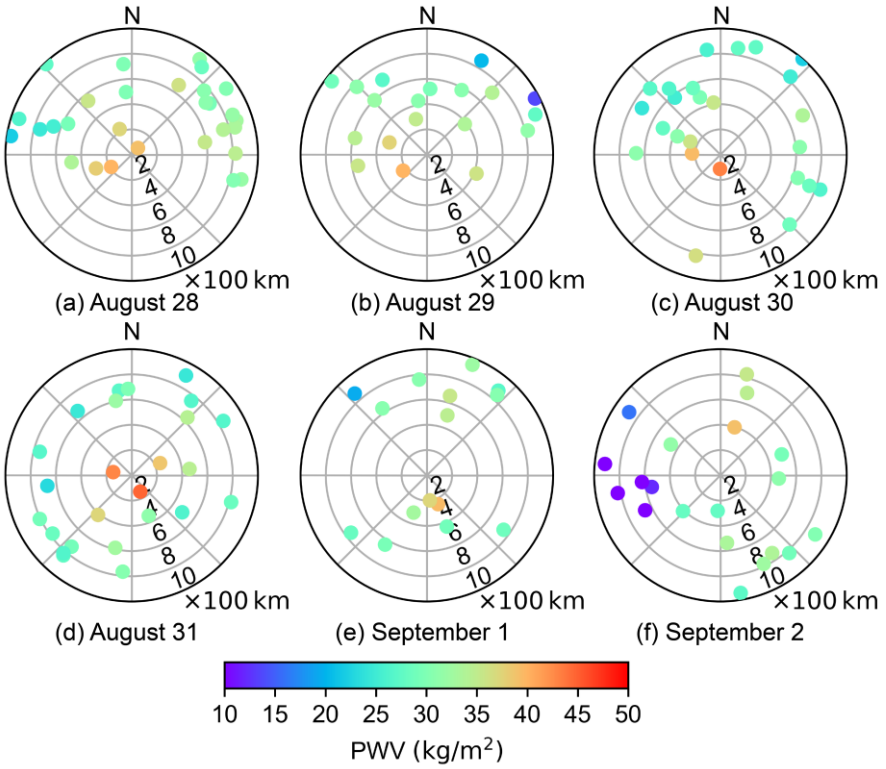

Fig. 2 The distribution of GNSS RO sounding points within a radius of 1,000 km from the TC center during the period from August 28 to September 2, 2020. The center of each plot represents the TC center

The detailed statistics of PWV on each day are listed in Table 1. The daily mean PWV was stable around ~30.0 kg/m^2 during the TC developing period of August 28 to September 1. On September 2, the mean PWV was much lower 15.2 kg/m^2, because no RO observations within a radius of 200 km from TC center.

Table 1 PWV daily statistics from August 28 to September 2, 2020. The 1-minute maximum sustained surface wind speed at 00:00 UT on each day is shown in the last column. The numbers in parentheses denote the number of soundings from GNSS RO missions COSMIC-2, Metop-A, Metop-B, Metop-C, KOMPSAT5, PAZ, TSX, TDX

Date	Max. PWV (kg/m^2)	Min. PWV (kg/m^2)	Mean PWV (kg/m^2)	# of sounding points	Max. sustained wind speed (km/h) at 00:00 UT
August 28	40.0	22.0	31.7	29 (24,1,2,1,0,0,1,0)	46.3
August 29	39.9	13.7	31.0	19 (15,0,2,1,0,0,1,0)	100.0

August 30	43.2	22.2	29.9	25 (20,1,3,0,0,1,0,0)	129.6
August 31	44.7	23.0	30.5	25 (22,2,0,1,0,0,0,0)	172.2
September 1	39.5	19.5	31.0	15 (13,0,0,0,2,0,0,0)	213.0
September 2	39.1	7.5	15.2	20 (18,0,0,0,2,0,0,0)	194.5

We defined five bands with different radii from the TC center: 1) band 1 with the distance of 0–200 km; 2) band 2 with the distance of 200–400 km; 3) band 3 with the distance of 400–600 km; 4) band 4 with the distance of 600–800 km; 5) band 5 with the distance of 800–1,000 km, as shown in Fig. 3 (a). Then, the average PWV of GNSS RO sounding events located in each band during the whole TC period was calculated, and the results were shown in Fig. 3 (b). The results demonstrated that the PWV with a smaller radius distance had a larger value. The average PWV for band 1 increased from ~39.5 kg/m^2 to ~43.6 kg/m^2 during the period from August 28 to August 31. Then, it suddenly decreased to ~37.4 kg/m^2 on September 1. Compared with the variation of average PWV in band 1, the PWV in the other four bands experienced a generally decreasing trend during the TC period. The daily mean decrease rate is 0.82 (kg/m^2)·day^{-1}, 1.05 (kg/m^2)·day^{-1}, 1.28 (kg/m^2)·day^{-1}, and 1.63 (kg/m^2)·day^{-1} for band 2, band 3, band 4, and band 5, respectively. The results imply that the PWV with a larger distance from TC center had a larger PWV decrease rate.

The daily mean PWV in each band was displayed in Fig. 3 (c). A clear decreasing trend was observed. The PWV monotonously decreased from the band 1 (inner band closest to TC center) to band 5 (outside band furthest from the TC center). The mean PWV in the band 1 is about 41.0 kg/m^2 and it decreased to about 26.5 kg/m^2 in band 5. The mean slopes between each neighbor band was -2.47 $kg \cdot m^{-2} \cdot (100km)^{-1}$ between band 1 and band 2, -2.27 $kg \cdot m^{-2} \cdot (100km)^{-1}$ between band 2 and band 3, -1.17 $kg \cdot m^{-2} \cdot (100km)^{-1}$ between band 3 and band 4, and -1.16 $kg \cdot m^{-2} \cdot (100km)^{-1}$ between band 4 and band 5. This result implied that the PWV in bands closer to the TC center had a larger spatial gradient than PWV in bands far away from TC center. By the way, on September 2, the PWV showed a low level in each band when the TC intensity started to decrease.

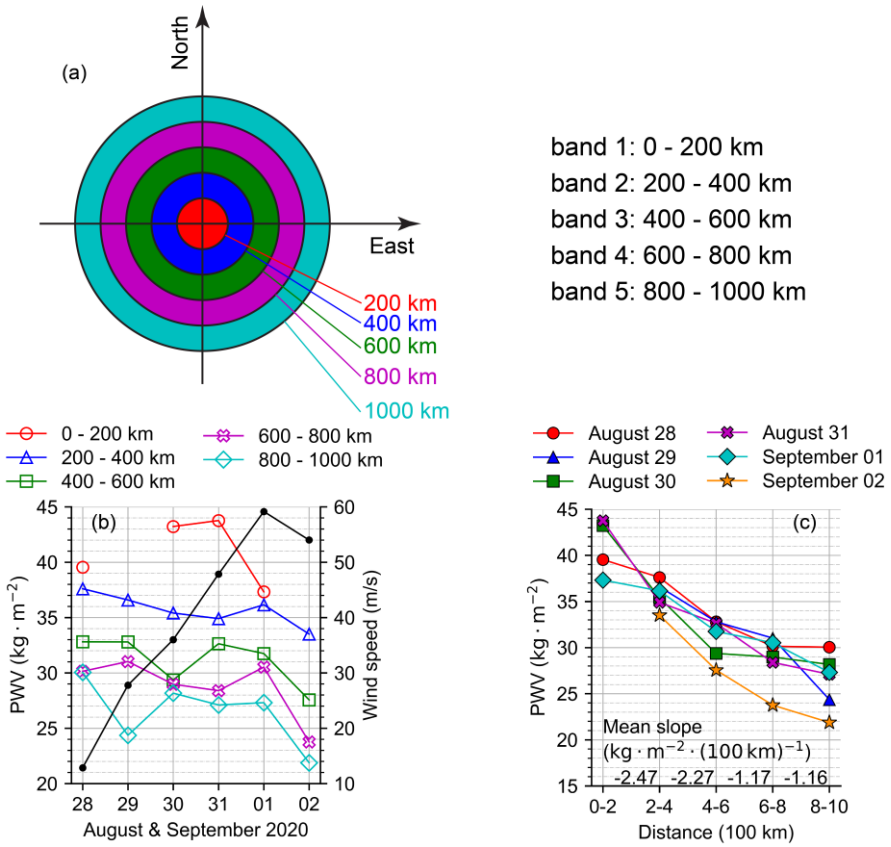

Fig. 3 Mean PWV in different bands during the TC period from August 28 to September 2, 2020. (a) the definition of five bands: band 1 is the region within a radius of 0–200 km from TC center; band 2 for 200–400 km; band 3 for 400–600 km; band 4 for 600–800 km; and band 5 for 800–1000 km; (b) PWV temporal variations in each band against the maximum sustained wind speed (black line with dots); (c) PWV variation in each band and the spatial change rate between two adjacent bands with respect to the PWV distance from TC center, during the TC period from August 28 to September 2, 2020. The PWV over the altitudes from 1.6 km to 40.0 km was used for the calculation

3.2 PWV Variation based on Altimetry Satellite Soundings

During the TC period, four PWV sounding tracks of the altimetry satellites passed through the TC area, as shown in Fig. 4. The first PWV pass was from the altimetry satellite mission SARAL, as shown in Fig. 4 (a). At ~ 21:00 UT on August 30, 2020, the SARAL PWV observations had the closest distance to TC, ~245 km. The second PWV pass was from the altimetry satellite mission Sentinel 3A, as shown in Fig. 4 (b). The PWV was measured at ~ 01:50 UT on August 31. The shortest distance between the sounding track and the TC center was ~256 km. The altimetry satellite

mission Jason-3 provided the third PWV pass at ~ 07:30 UT on August 31, as shown in Fig. 4 (c). The closest distance between the PWV pass and the TC center was ~164 km. The last PWV pass with the closest distance of ~161 km from the TC center was sounded by the altimetry satellite mission Sentinel 3B at ~02:00 UT on September 2, as shown in Fig. 4 (d).

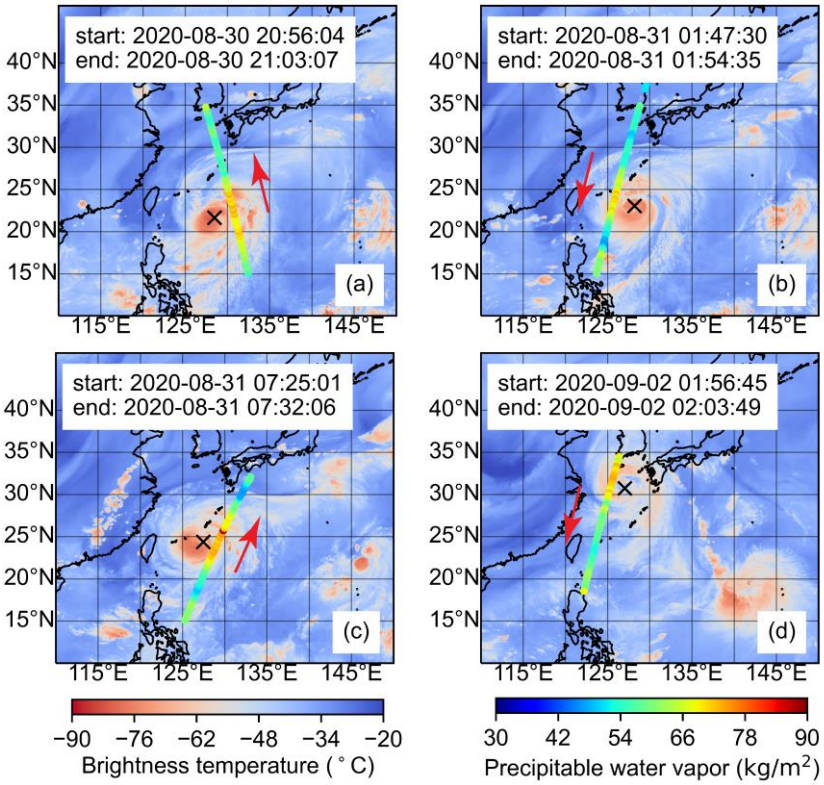

Fig. 4 The PWV sounding points from different altimetry satellite missions: (a) SARAL; (b) Sentinel 3A; (c) Jason-3; (d) Sentinel 3B. The cross marker was the location of the TC eye center. The red arrow denoted the flying direction of the altimetry satellite. The background color denoted the brightness temperature, which was retrieved from the Japanese Himawari-8 satellite products

The PWV variation along the sounding tracks is shown in Fig. 5. The PWV showed a significant increase when the sounding points got closer to the TC center. The PWV started to increase from a distance of ~600 km from the TC center. At such a distance, the PWV over the four passes was around 50 kg/m^2 on average. The rich PWV could be observed near the TC center, i.e. ~78.0 kg/m^2 in the first pass, ~73.4 kg/m^2 in the second pass, ~90.1 kg/m^2 in the third pass, and ~75.4 kg/m^2 in the fourth pass. Furthermore, we conducted a linear regression for the PWV sounding points within a distance of 600 km from the TC center, including altimetry

satellite soundings approaching to and departing from TC center. The results showed that the slopes of the linear regression function, $f(x) = a \cdot x + b$, during the approaching and departing phases were generally symmetric around the TC center in all the four passes. In detail, the slopes of the first pass during the approach and departing phases were 0.0253 $kg \cdot m^{-2} \cdot km^{-1}$ and -0.0312 $kg \cdot m^{-2} \cdot km^{-1}$, respectively; 0.0524 $kg \cdot m^{-2} \cdot km^{-1}$ and -0.0685 $kg \cdot m^{-2} \cdot km^{-1}$ in the second pass, 0.0574 $kg \cdot m^{-2} \cdot km^{-1}$ and -0.0410 $kg \cdot m^{-2} \cdot km^{-1}$ in the third pass, and 0.0260 $kg \cdot m^{-2} \cdot km^{-1}$ and -0.0203 $kg \cdot m^{-2} \cdot km^{-1}$ in the fourth pass. It is worth noting the large slopes could be observed on August 31.

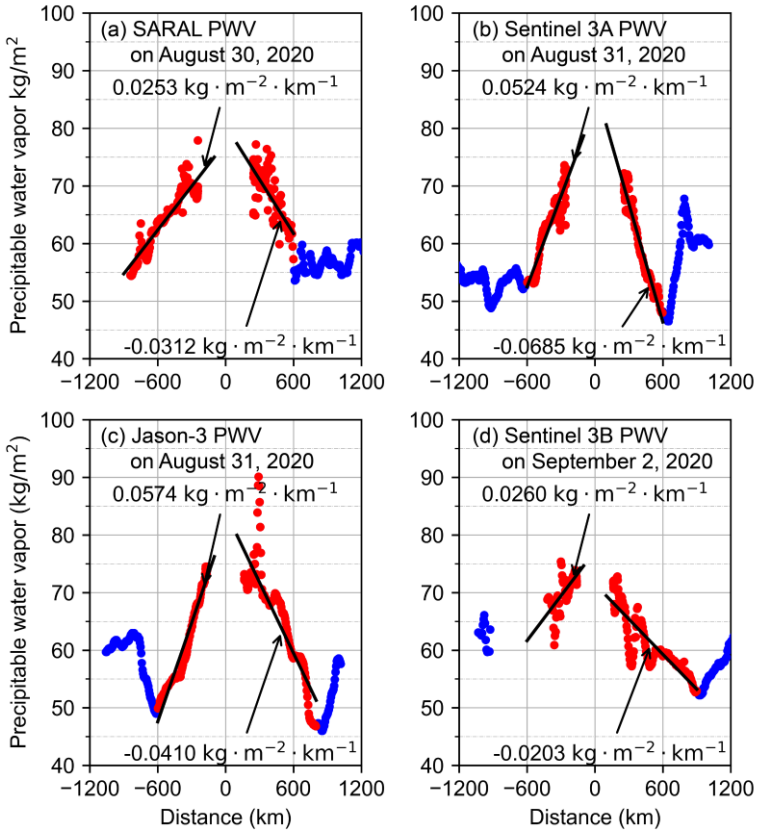

Fig. 5 Variation of PWV, denoted in blue dots, were retrieved from different altimetry satellite passes against the distance from the TC eye center: (a) PWV retrieved from SARAL during 20:56~21:03 UT on August 30, 2020; (b) PWV retrieved from Sentinel 3A during 01:47~01:54 UT on August 31, 2020; (c) PWV retrieved from Jason-3 during 07:25~07:32 UT on August 31, 2020; (d) PWV retrieved from Sentinel 3B during 01:56~02:03 UT on September 02, 2020. The location of PWV observations approaching toward or departing from the TC center was shown with a negative or positive distance, respectively. The PWV data used for linear regression, i.e. $f(x) = a \cdot x + b$, was depicted as red dots

4 Conclusions

The PWV variation during the TC period was investigated based on both GNSS RO and satellite microwave radiometer data. The main findings were:

1. The PWV experienced a significant increase when the location is closer to the TC center during the TC period, while the PWV showed a decreasing trend when the location is further from the TC center.
2. In the radial direction, the PWV gradient between each 200-km-interval band was -2.47 $kg \cdot m^2 \cdot (100km)^{-1}$ between band 1 (within ~200 km from TC center) and band 2 (200–400 km from TC center), -2.27 $kg \cdot m^2 \cdot (100km)^{-1}$ between band 2 and band 3 (400–600 km from TC center), -1.17 $kg \cdot m^2 \cdot (100km)^{-1}$ between band 3 and band 4 (600–800 km from TC center), and -1.16 $kg \cdot m^2 \cdot (100km)^{-1}$ between band 4 and band 5 (800–1,000 km from TC center).
3. The PWV clearly showed a spatially symmetric distribution around the TC center, as revealed from the PWV data of altimetry satellites. The PWV spatial increase gradient during the satellite approaching to TC center and spatial decrease gradient during satellite departing from TC center were 2.53 $kg \cdot m^2 \cdot (100km)^{-1}$ and -3.12 $kg \cdot m^2 \cdot (100km)^{-1}$, respectively, as retrieved from SARAL PWV on August 30, 5.24 $kg \cdot m^2 \cdot (100km)^{-1}$ and -6.85 $kg \cdot m^2 \cdot (100km)^{-1}$, respectively, as retrieved from Sentinel 3A PWV on August 31, 5.74 $kg \cdot m^2 \cdot (100km)^{-1}$ and -4.10 $kg \cdot m^2 \cdot (100km)^{-1}$, respectively, as retrieved from Jason-3 PWV on August 31, and 2.60 $kg \cdot m^2 \cdot (100km)^{-1}$ and -2.03 $kg \cdot m^2 \cdot (100km)^{-1}$, respectively, as retrieved from Sentinel 3B PWV on September 2.

Acknowledgments

The grant support from the Key Program of the National Natural Science Foundation of China (project No.: 41730109) is acknowledged. The grant supports from the Hong Kong Research Grants Council (RGC) project (B-Q61L PolyU 152222/17E) are highly appreciated. The support from the project (No. 1-BBWJ) in the Emerging Frontier Area (EFA) Scheme of Research Institute for Sustainable Urban Development (RISUD) of The Hong Kong Polytechnic University is also acknowledged.

References

1. Marks FD (2015) Tropical Cyclones And Hurricanes | Hurricanes: Observation. In: North GR, Pyle J, Zhang F (eds) Encycl. Atmospheric Sci. Second Ed. Academic Press, Oxford, pp 35–56
2. Mendelsohn R, Emanuel K, Chonabayashi S, Bakkensen L (2012) The impact of climate change on global tropical cyclone damage. Nat Clim Change 2:205–209
3. Bakkensen LA, Mendelsohn RO (2019) Global Tropical Cyclone Damages and Fatalities Under Climate Change: An Updated Assessment. In: Collins JM, Walsh K (eds) Hurric. Risk. Springer International Publishing, Cham, pp 179–197

4. Yamaguchi M, Chan JCL, Moon I-J, Yoshida K, Mizuta R (2020) Global warming changes tropical cyclone translation speed. Nat Commun 11:47
5. Keclik AM, Evans C, Roebber PJ, Romine GS (2017) The influence of assimilated upstream, preconvective dropsonde observations on ensemble forecasts of convection initiation during the Mesoscale Predictability Experiment. Mon Weather Rev 145:4747–4770
6. Lu Q, Hu J, Wu C, et al (2020) Monitoring the performance of the Fengyun satellite instruments using radiative transfer models and NWP fields. J Quant Spectrosc Radiat Transf 255:107239
7. Draper DW, Newell DA, Wentz FJ, Krimchansky S, Skofronick-Jackson GM (2015) The Global Precipitation Measurement (GPM) Microwave Imager (GMI): Instrument Overview and Early On-Orbit Performance. IEEE J Sel Top Appl Earth Obs Remote Sens 8:3452–3462
8. Healy SB, Polichtchouk I, Horányi A (2020) Monthly and zonally averaged zonal wind information in the equatorial stratosphere provided by GNSS radio occultation. Q J R Meteorol Soc 146:3612–3621
9. Bai W, Deng N, Sun Y, et al (2020) Applications of GNSS-RO to Numerical Weather Prediction and Tropical Cyclone Forecast. Atmosphere. https://doi.org/10.3390/atmos11111204
10. Mueller MJ, Kren AC, Cucurull L, Casey SP, Hoffman RN, Atlas R, Peevey TR (2020) Impact of refractivity profiles from a proposed GNSS-RO constellation on tropical cyclone forecasts in a global modeling system. Mon Weather Rev 148:3037–3057
11. Schreiner WS, Weiss JP, Anthes RA, et al (2020) COSMIC-2 Radio Occultation Constellation: First Results. Geophys Res Lett 47:e2019GL086841
12. Fernandes MJ, Lázaro C, Vieira T (2021) On the role of the troposphere in satellite altimetry. Remote Sens Environ 252:112149
13. Hong Kong Observatory (2020) Tropical Cyclones in 2020. Hong Kong Observatory, Hong Kong
14. Knapp KR, Kruk MC, Levinson DH, Diamond HJ, Neumann CJ (2010) The International Best Track Archive for Climate Stewardship (IBTrACS). Bull Am Meteorol Soc 91:363–376
15. Böhm J, Schuh H (2013) Atmospheric effects in space geodesy. Springer
16. Donlon C, Berruti B, Buongiorno A, et al (2012) The Global Monitoring for Environment and Security (GMES) Sentinel-3 mission. Sentin Missions - New Oppor Sci 120:37–57
17. Zhu M, Liu Z, Hu W (2020) Observing Water Vapor Variability During Three Super Typhoon Events in Hong Kong Based on GPS Water Vapor Tomographic Modeling Technique. J Geophys Res Atmospheres 125:e2019JD032318